Real-time Hardware-in-the-Loop Evaluation of a Partially Turboelectric Propulsion Control Design

Donald L. Simon*, Santino J. Bianco†
NASA Glenn Research Center, Cleveland, Ohio, 44135, USA

Marcus A. Horning‡
HX5, LLC, Brook Park, Ohio, 44142, USA

Joseph R. Saus§, Aria E. Amthor**, Jonah J. Sachs-Wetstone††
NASA Glenn Research Center, Cleveland, Ohio, 44135, USA

In support of aviation fuel burn and emission reduction goals, NASA is pursuing high-payoff research investments that promise to transform aviation. This includes investments in Electrified Aircraft Propulsion (EAP). Multiple technology challenges must be addressed to unlock the full potential of EAP. This includes addressing challenges related to propulsion controls, which will be vital for ensuring efficient coordinated operation of EAP subsystems. This paper presents results from real-time hardware-in-the-loop testing of a control design for a single aisle partially-turboelectric aircraft propulsion concept conducted at the NASA Electric Aircraft Testbed (NEAT) facility. The control system under test is designed for a propulsion concept consisting of two wing-mounted turbofan engines that produce thrust and generate electrical power to drive a boundary layer ingesting tailfan propulsor via an electrical motor. An integrated control strategy is applied to ensure coordinated operation of the turbofan and tailfan subsystems during steady-state and transient operation throughout the flight envelope. The NEAT test of this integrated control design consists of a partially hardware-in-the-loop, partially simulated configuration. A subscale representation of the electrical system design is implemented in hardware and mechanically coupled to electric machines that emulate turbomachinery and propulsor shaft dynamics. The hardware configuration is then operated under the control of a real-time computer application that runs a simulation of the propulsion system and the developed control logic. The NEAT facility test campaign includes a series of experiments that subject the control design to throttle transients conducted throughout the flight envelope and full-flight mission profiles. Testing under simulated performance degradation is also conducted to evaluate control design robustness. This includes constant and abrupt changes in degradation levels. Results from the hardware-in-the-loop test are presented and shown to be in good agreement with pre-test simulation predictions demonstrating the efficacy of the integrated control design approach.

* Control Systems Engineer, Intelligent Control and Autonomy Branch.
† Control Systems Engineer, Intelligent Control and Autonomy Branch, and AIAA member.
‡ Aerospace Engineer, HX5, LLC.
§ Control Systems Engineer, Intelligent Control and Autonomy Branch, and AIAA senior member.
** Control Systems Engineer, Intelligent Control and Autonomy Branch, and AIAA member.
†† Control Systems Engineer, Intelligent Control and Autonomy Branch, and AIAA member.

I. Nomenclature

CAN	= controller area network
DC	= direct current
EAP	= electrified aircraft propulsion
EoL	= end-of-life
EGT	= exhaust gas temperature
GUI	= graphical user interface
hp	= horsepower
HPC	= high pressure compressor
LP	= low pressure
kW	= kilowatt
LPC	= low pressure compressor
MIMO	= multi-input multi-output
MW	= megawatt
N_{1c}	= turbofan corrected fan speed
$\dot{N}_{1c}$	= turbofan corrected fan speed acceleration
N_{2c}	= turbofan corrected low pressure shaft speed
N_{3c}	= turbofan corrected core speed
N_{tc}	= tailfan corrected fan speed
NEAT	= NASA Electric Aircraft Testbed
NPSS	= Numerical Propulsion System Simulation
nm	= nautical mile
PLA	= power lever angle
PI	= proportional integral
Q_{cmd}	= tailfan motor commanded torque
SISO	= single-input single-output
SLS	= sea level static
SMICS	= Sliding Mode Impedance Controller with Scaling
STARC-ABL	= Single-aisle Turboelectric AiRCraft with Aft Boundary Layer propulsor
T-MATS	= toolbox for the modeling and analysis of thermodynamic systems
VAFN	= variable area fan nozzle
VBV	= variable bleed valve
w_f	= fuel flow rate
$w_{f,cmd}$	= turbofan commanded fuel flow rate

II. Introduction

Under the Sustainable Flight National Partnership, NASA is engaging with other federal agencies, industry, and academia to accomplish the aviation community's goal of net-zero carbon emissions by 2050 [1]. A major technology emphasis is Electrified Aircraft Propulsion (EAP), which relies on the generation, storage, transmission, and/or use of electrical power for producing thrust [2,3,4]. EAP enables the design of revolutionary propulsion architectures that hold great potential for supporting the sustainable aviation goals of fuel burn and emissions reduction. This includes designs that combine gas turbine engines with electrical system hardware. Multiple technology challenges must be addressed to unlock the full potential of EAP. In particular, advances in propulsion controls will be vital for ensuring coordinated efficient operation of the complex integrated subsystems that comprise EAP architectures.

An example EAP concept is the Single-aisle Turboelectric AiRCraft with Aft Boundary Layer propulsor (STARC-ABL) shown in Fig. 1. The STARC-ABL is a partially-turboelectric concept aircraft proposed by NASA [5,6]. It has two wing-mounted turbofan engines and an electric motor-driven boundary layer ingestion tailfan propulsor. The turbofans serve the dual purpose of generating thrust and supplying mechanical offtake power that is converted to electricity and delivered to the tailfan motor over a high voltage direct current (DC) power bus. The STARC-ABL exhibits

Figure 1. STARC-ABL Aircraft

electromechanical coupling between its turbofan and tailfan subsystems and requires an integrated control strategy to ensure optimal efficiency and operability. Past NASA publications covering control design for the STARC-ABL propulsion system are found in Refs. [7,8,9]. These efforts took the approach of either designing separate closed-loop controllers for the turbofan and tailfan subsystems in an ad hoc decentralized fashion [7,8] or operating the tailfan under open-loop control [9]. Both approaches have their limitations. The decentralized control approach requires a tedious design effort to achieve coordinated subsystem operation during transients and is prone to operability concerns during rapid throttle movements. The open-loop control approach sacrifices the ability to tightly control tailfan thrust output. To address these shortcomings, Ref. [10] introduces a new integrated control design strategy for the STARC-ABL that directly accounts for the coupling between the turbofan and tailfan subsystems. This approach promotes operability, enables tighter control of thrust, and has been found to simplify the overall control design effort.

This paper will present results from a real-time hardware-in-the-loop test of the STARC-ABL integrated control design introduced in Ref. [10]. The test was conducted at the NASA Electric Aircraft Testbed (NEAT), a facility that enables testing of megawatt (MW)-level electric aircraft power systems [11]. The NEAT test enabled the performance of the STARC-ABL integrated control design to be evaluated when controlling actual electrical system hardware. This included evaluation of the control design's robustness to variations in throttle input, flight condition, and simulated turbomachinery performance degradation.

The remaining sections of this paper will discuss the development and NEAT facility testing of the STARC-ABL integrated control design. Section III provides an overview of the STARC-ABL propulsion system and the integrated control design developed for it. Section IV discusses the test configuration of the STARC-ABL electrical system implemented in the NEAT facility for the testing of the developed control design. Sections V and VI discuss the test matrix and test results, respectively. Conclusions are presented in Section VII.

III. STARC-ABL Propulsion Architecture and Control Design

The STARC-ABL exhibits the electromechanical coupling between subsystems inherent in many EAP designs making it a good candidate for conducting EAP integrated controls research. A depiction of the STARC-ABL concept and its mechanical-electrical architecture is shown in Fig. 2. Electric generators are connected to the low-pressure (LP) shaft of each turbofan and are configured to supply power to a constant voltage DC bus. Connected to this same DC bus is a 3500-horsepower (hp) electric motor used to drive the tailfan. The STARC-ABL poses a multi-input multi-output (MIMO) control design problem in the sense that there are multiple inputs (fuel flow rate and motor torques) used to control multiple outputs (turbofan and tailfan corrected fan speeds). The overall system requires an integrated control strategy to allow individual subsystems to transiently respond to changing throttle commands in a coordinated fashion.

The original publications introducing the STARC-ABL concept (see Refs. [5,6]) are system studies focused on exploring the efficiency and design space offered by partially-turboelectric EAP architectures. These references only consider operation of the STARC-ABL's turbofan and tailfan subsystems from a steady-state perspective, and do not explicitly specify a transient control concept of operations. There are two primary options for controlling the transfer of electrical power in the STARC-ABL's electrical system while striving to hold a constant DC bus voltage. The first option is to command the generators to deliver a specified amount of power to the bus while controlling the tailfan motor to consume power at the rate necessary to hold the bus voltage constant. This will result in a forward-to-aft coupling in the electrical system where operation of the tailfan is dependent on the amount of generated power supplied by the turbofans. A drawback of this option is that it forces the tailfan to be operated open-loop, which sacrifices the

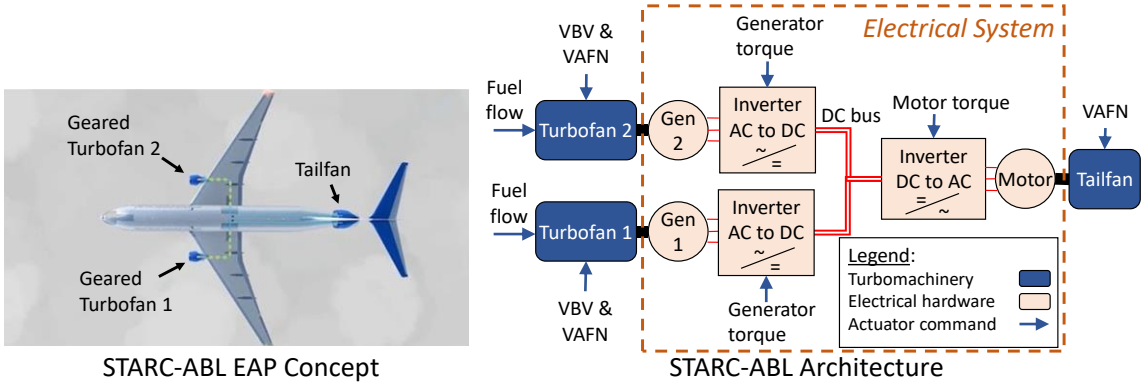

Figure 2. STARC-ABL Turboelectric Propulsion Concept and Architecture

ability to precisely control tailfan thrust output. The second option is to operate the tailfan motor under closed-loop control while relying on the generators to act as the bus voltage regulators. This results in an aft-to-forward coupling in the electrical system where any change in the tailfan motor power demand will result in a corresponding change in the amount of power the generators must extract from the turbofans to hold the bus voltage constant. The coupling option enables more precise control of vehicle net thrust output. It allows direct control of tailfan thrust using motor torque inputs and as well as turbofan thrust using fuel flow rate inputs. This aft-to-forward bus voltage regulation strategy is the control approach taken in this effort.

In addition to the motor, generators, and turbofan fuel metering valves, additional STARC-ABL control actuators include a variable bleed valve (VBV) and variable area fan nozzle (VAFN) installed on each of the two geared turbofan engines, and an additional VAFN on the tailfan. The VBVs and VAFNs operate under open-loop control schedules.

A. STARC-ABL Integrated Control Design

For a detailed description of the STARC-ABL integrated control design developed under this effort, readers are referred to Ref. [10]. A block diagram of the STARC-ABL and the developed control system is shown in Fig. 3. Each turbofan has a proportional integral (PI) fuel controller that produces a fuel flow rate command, $w_{f,cmd}$, based on the error between commanded corrected fan speed, $N_{1c,cmd}$, and sensed corrected fan speed, N_{1c}. The tailfan has a PI motor controller that produces a motor torque command, Q_{cmd}, based on the error between commanded corrected tailfan speed, $N_{tc,cmd}$, and sensed corrected tailfan speed, N_{tc}. The commanded speed setpoints for the turbofans and tailfan are provided by the power management schedule blocks shown in the figure. The power management schedules define the commanded speed setpoints based on cockpit throttle position and flight condition. They are implemented as multi-dimensional lookup tables that accept inputs of altitude, Mach number, and throttle angular position (denoted as power lever angle (PLA)) and produce corrected speed setpoint outputs. Corrected fan speed, which closely correlates with net thrust, is commonly used as a proxy for thrust when designing aircraft engine controls due to the challenge of accurately measuring thrust in-flight [12]. The pilot has the ability to command the full-range STARC-ABL net thrust settings from idle to maximum power through PLA adjustments. The bus voltage controller shown in Fig. 3 induces the coupling that tailfan electrical power demand places on the operation of the turbofans. This controller is envisioned to be a closed-loop design where adjustments to commanded generator power output are made to hold a target DC bus voltage. However, for the analysis performed in this study the effect of the bus voltage controller is captured as a simple feedback parameter as opposed to implementing an actual closed-loop control design with dynamics. This simplification is possible as the dynamics of this electrical system controller are assumed to occur at a time scale significantly faster than turbomachinery dynamics. Given this assumption, the coupling effect induced by the bus voltage controller is captured by calculating the total instantaneous power consumed by the tailfan motor plus electrical system efficiency and resistive losses, and then commanding each generator to deliver half of this amount of power. Under most operating conditions, the thrust schedules result in the generators extracting approximately 28% of the total power delivered to the LP shaft of each turbofan by its low-pressure turbine. This level

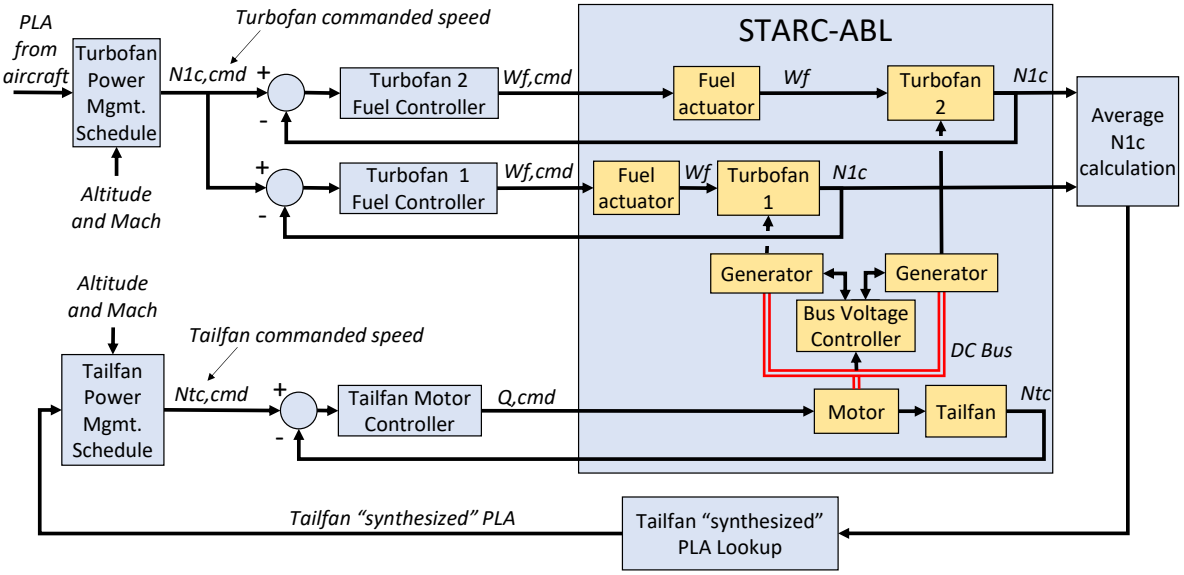

Figure 3. STARC-ABL Integrated Control Architecture

of power extraction allows the steady-state operating line of the turbofans to reside near a region of peak efficiency, particularly when operating at cruise conditions. The 28% power extraction level is maintained at all operating conditions where the tailfan motor remains below its maximum 3500hp limit. However, high PLA settings at low to intermediate altitudes will result in the tailfan reaching the 3500hp limit. This will restrict tailfan speed and thrust output. Under such conditions, increasing PLA beyond the point where the motor limit is encountered will cause an increase in turbofan speed and thrust output while the tailfan motor speed and thrust remains "plateaued" at the limit.

A key aspect of the integrated control design approach is the implementation of a single PLA throttle command from the aircraft (see Fig. 3). This is a departure from conventional commercial aircraft vehicle-propulsion interface designs where separate throttle inputs are available to independently control the operation of each engine installed on the vehicle. The single throttle approach is implemented here to guard against uncoordinated operation of the turbofan and tailfan subsystems. A notional illustration of this concern is depicted in Fig. 4a. Shown are normalized fan speed responses for the turbofans and the tailfan assuming that all subsystem controllers receive an identical PLA input consisting of a step increase followed by a step decrease. While tedious, it is possible to design separate turbofan and tailfan controllers that provide an acceptable acceleration response. This results in the subsystems exhibiting similar speed response during the initial portion of the acceleration transient followed by the turbofans continuing to accelerate after the tailfan plateaus at its maximum motor power limit, as shown in Fig. 4a. However, a potential problem arises on the PLA step decrease. Here, the tailfan leads the turbofans in the deceleration due to its lower plateauing speed starting point. This results in the rapid unloading of the turbofan LP shaft through reduced power extraction. This poses an elevated risk of potential turbofan compressor stalls. The solution applied to address this transient mismatch concern is to calculate and supply a "synthesized" PLA command input signal to the tailfan power management schedule. The synthesized PLA command is a function of the average sensed N_{1c} of the two turbofans and equates to the PLA setting that would produce that same N_{1c} under steady-state conditions. Applying the tailfan synthesized PLA promotes better synchronized operation of the turbofan and tailfan subsystems as shown in Fig. 4b. Here, the tailfan and turbofan subsystems exhibit coordinated responses during both acceleration and deceleration transients.

An acknowledged limitation of the single PLA approach is that it does not permit the STARC-ABL's two turbofan engines to be controlled in an independent fashion. Although not analyzed as part of this study, an alternative vehicle-propulsion interface that includes separate PLA inputs for the left and right turbofan should be possible. Such an approach would require a more complex control strategy accounting for asymmetric operation of the turbofans and their generator power offtake levels. This is an area recommended for potential follow-on research and evaluation.

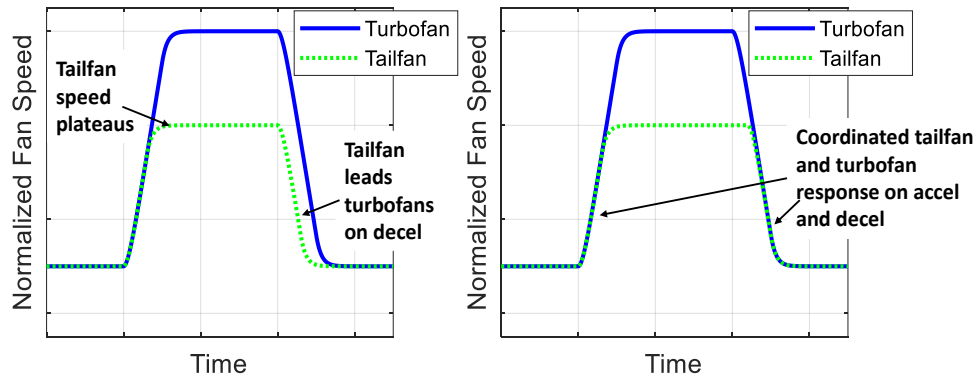

Figure 4: Notional Illustration of Turbofan and Tailfan Transient Operation

Implementation of the "synthesized" tailfan PLA results in direct coupling of the dynamic operation of the STARC-ABL tailfan and turbofan subsystems. As detailed in Ref. [10], this enables derivation of the linear transfer function given in Eq. (1).

$$\frac{N_{1c}(s)}{w_f(s)} = \frac{K_e(s+z_1)}{[(s+r_1)(s+r_2) - H(s)]} \tag{1}$$

This single-input single-output (SISO) transfer function relates turbofan fuel flow rate input, w_f, to turbofan N_{1c} output. The $\frac{K_e(s+z_1)}{[(s+r_1)(s+r_2)]}$ portion of Eq. (1) is equivalent to the open-loop transfer function of a two-spool turbofan

engine with poles r_1 and r_2, zero z_1, and transfer function gain, K_e [12]. The $H(s)$ transfer function in the denominator captures the tailfan motor-induced generator power extraction dynamics placed on the LP shaft of the turbofans. $H(s)$ is a function of both tailfan and turbofan dynamics as well as tailfan motor PI control gains.

PI setpoint controllers are designed for the tailfan and turbofans at operating points spanning a range of altitudes, Mach numbers, and power levels covering the STARC-ABL flight envelope. At each operating point, control design occurs in a two-step process. First, PI gains for the tailfan motor controller are chosen to produce a desired tailfan closed-loop response. The resulting tailfan control gains are then combined with linear model parameters to produce Eq. (1) and PI gain selection for the turbofan fuel controller proceeds. This second step of selecting turbofan fuel control gains based on Eq. (1) has been found to simplify the overall control design process compared to previous approaches presented in Refs. [7,8]. Previous approaches required more back-and-forth iteration between tailfan and turbofan control gain selection to produce an acceptable control response. Use of Eq. (1) reduces the need for such design iterations and enables direct application of classical linear control design analysis techniques such as bode diagrams or pole-zero maps [10,12]. In addition to the PI setpoint controllers, acceleration and deceleration control schedules based on turbofan corrected fan speed acceleration, $\dot{N}_{1c}$, are also developed along with limit logic designed to limit maximum tailfan motor power and minimum turbofan high pressure compressor exit pressure. The resulting control designs at each operating point are combined in a piecewise linear schedule. Switching between control modes is performed by conventional maximum-minimum mode selection logic, which selects the active control regulator at any instant in time [12]. This forms a full-flight envelope controller for the STARC-ABL propulsion system that provides the desired synchronized operation of the turbofans and the tailfan during any PLA command including rapid PLA transients.

B. Pre-Test Simulation Analysis

Controls development was performed using a nonlinear transient model of the STARC-ABL propulsion system. This model was derived from a steady-state model coded in the Numerical Propulsion System Simulation (NPSS) environment [13]. The NPSS model was converted to the MATLAB® Simulink® (MathWorks, Natick, MA) environment using the NASA-developed Toolbox for the Modeling and Analysis of Thermodynamic Systems (T-MATS) [14] and a power flow modeling approach [15]. T-MATS is applied to model the turbomachinery components and the power flow modeling approach is used to model electrical system components at turbomachinery time-scales. Shaft dynamics and a transient solver are also included to enable simulation of transient operation. The resulting model supports the generation of linear state-space models for control design purposes. The completed control design paired with the nonlinear model yields a full-flight envelope closed-loop model.

The closed-loop STARC-ABL model played a key role in preparing for the NEAT facility test. All test scenarios planned for evaluation during the test campaign underwent a pre-test simulation analysis using the model. This enabled evaluation and refinement of the control design to ensure that desired system performance and operability was maintained over all planned test scenarios.

IV. NEAT Facility Configuration

To evaluate the performance of the STARC-ABL control design when exposed to actual electric system hardware and noise levels, a real-time hardware-in-the-loop test was conducted at the NEAT facility located at the NASA Glenn Research Center Neil A. Armstrong Test Facility. NEAT is a reconfigurable testbed used to design, develop, assemble, and test MW-level electric aircraft power systems [11]. Photographs of the NEAT facility, electrical system hardware, and the control room are shown in Fig. 5. Figure 6 provides a diagram showing the NEAT STARC-ABL test configuration, which consists of both actual hardware and simulated components.

Figure 5. NEAT Facility Exterior, Electrical System Hardware, and Control Room

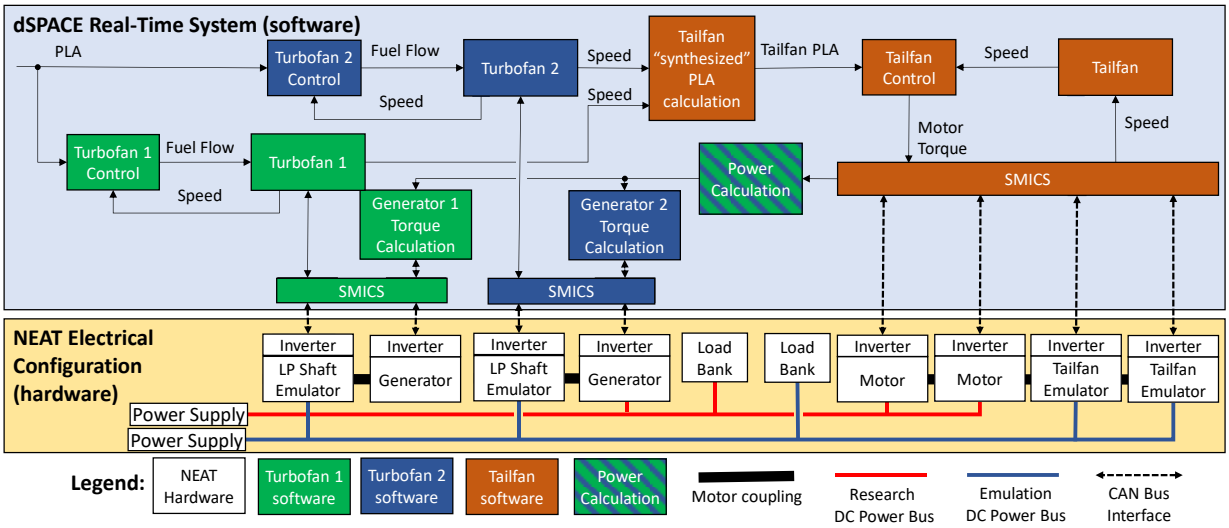

Figure 6. NEAT STARC-ABL Controls Test Configuration

A. NEAT Electrical System Hardware Configuration

Electrical system hardware, which is shown in the bottom half of Fig. 6, is configured to represent a subscale version of the STARC-ABL electrical system and the turbofan and propulsor shaft dynamics. This includes eight 250 kilowatt (kW) electric machines, each equipped with an inverter. The motors and inverters are liquid cooled by a facility chiller system. The electric machines are mechanically coupled to represent three separate rotating shafts: turbofan 1 LP shaft, turbofan 2 LP shaft, and the tailfan shaft. The two turbofan LP shaft representations consist of electric machine pairs, where one electric machine emulates turbofan LP shaft dynamics and the second electric machine operates as a generator that would be interfaced with the LP shaft. The third shaft consists of four electric machines where two of the electric machines operate in tandem to emulate tailfan shaft dynamics while the remaining two electric machines operate in tandem to represent the tailfan motor. The 250kW electric machines used at the NEAT facility are smaller than those required for the full-scale STARC-ABL propulsion system. Because of this, a subscale version of the electrical system hardware is implemented at NEAT that operates at approximately 9% of the 2.7MW full-scale power level of the STARC-ABL. The experimental configuration at the NEAT facility includes two DC electrical power buses, both supplied by unidirectional DC power supplies. Electric machines that represent subscale versions of the STARC-ABL motor and generators are connected to the research bus (shown in red in Fig. 6) while electric machines used to emulate turbomachinery and propulsor shaft dynamics are connected to the emulation bus (shown in blue in Fig. 6). Adjustable load banks are also included on each bus to guard against reverse power flow during the test. After assembly of the NEAT STARC-ABL controls test configuration, measurements were taken to ensure proper bonding and grounding of the system before commencing the test campaign. The system also includes an array of circuit breaker, ground fault monitoring hardware, and facility instrumentation that was monitored during the test.

B. NEAT Software Configuration

Remaining elements of the STARC-ABL propulsion system model and the integrated control design are implemented in software as shown in the top half of Fig. 6. To test the control design at NEAT without modification, several differences between the full-scale STARC-ABL and subscale NEAT electrical systems are addressed. This includes differences in rated power levels, speeds, and torques of the electric machine as well as differences in rotational shaft inertia and viscous damping. To address these inconsistencies, an innovative sliding mode impedance controller with scaling (SMICS) approach is applied [16]. SMICS provides two enabling features. First, it directs operation of the electric machines by scaling torque commands supplied to the motor inverters and unscaling speed feedback measurements passed back to the STARC-ABL model. This allows NEAT electric machines to operate within their torque and speed operating limits. Second, SMICS applies a nonlinear discontinuous closed-loop control strategy to direct operation of the electric machines tasked with emulating turbomachinery shafts. This allows the emulation electric machines to robustly mimic a subscale representation of the shaft dynamics as prescribed by the model.

While SMICS provides power scaling and shaft dynamics emulation functionality, it does not account for efficiency differences between the NEAT motor/inverter hardware versus that of STARC-ABL. This is significant as the overall control design is developed assuming that the efficiencies specified for the STARC-ABL concept in Refs. [5,6] are correct. If the generators are operating to hold a constant DC bus voltage, these efficiency differences will result in an "off-schedule" amount of power extracted from the turbofans. This will cause the turbofan models and their controllers to operate in a manner inconsistent with their designs, which poses concerns regarding turbofan operability and the numerical stability of the models. To address this issue, the generators are not operated as bus voltage controllers. Instead, the software "power calculation" block shown in the top half of Fig. 6 is applied. Based on the operating speed and torque of the tailfan motor, the power calculation block calculates the corresponding amount of power that the generators should extract from the turbofans based on the efficiencies in Refs. [5,6]. This calculated power signal along with generator speeds is provided as input to the "generator torque calculation" blocks, which calculate the appropriate torque commands supplied to the generators. In combination, the SMICS algorithm and the power calculation block allow the full-scale STARC-ABL integrated control design to undergo testing without modification or the inclusion of physical gas turbine hardware. Due to the software solution applied to address the mismatch in electrical system efficiencies, the amount of DC bus power produced by the generators will not exactly match the power consumed by the tailfan motor. This potential excess or deficit in bus power consumption is addressed through the inclusion of the load banks, which guard against reverse power flow into the power supplies.

Available motor data from NEAT facility testing conducted prior to the STARC-ABL controls test indicated that the motor speed feedback measurements exhibited a significant amount of measurement noise. To account for this, first order low-pass filtering of all speed feedback measurements is applied. The dynamics of this filtering is accounted for in the STARC-ABL integrated control design process.

C. Real-Time Software Application and Computer System

The STARC-ABL propulsion system and the integrated control design software are coded as a real-time application and implemented in a dSPACE SCALEXIO real-time computing system. The real-time application, which directs the operation of the electric motors, is employed to meet the strict time constraints required by the hardware-in-the-loop control test. This application is built using dSPACE ConfigurationDesk, which compiles the MATLAB and Simulink code related to the engine model, controller, and the command and data handling system. A graphical user interface (GUI), developed using dSPACE ControlDesk, allows the operator to send commands to the application, edit test-specific settings, check the status of faults and alarms, view telemetry from the test hardware, and display data from Simulink models processed in real-time.

A high-level state machine diagram illustrating the behavior of the real-time application during test operations is shown in Fig. 7. The application consists of three main states including "Stop," "Run," and "Fault." During startup, the application begins in the "Stop" state. An entry into this state will trigger the inverters to immediately disable. When the operator selects the appropriate button from the GUI, the application will transition from the "Stop" state to the "Run" state. Three user-selected modes are available in the "Run" state: manual mode, scripted mode, and automated mode. In manual mode the operator can directly command the motor mode of operation (torque control mode or speed control mode), the torque/speed commanded setpoint, and the inverter state (enabled or disabled). Scripted mode allows the operator to run a pre-programmed time-history sequence of motor commands. The manual and scripted operating modes were used during initial verification of system software and communication. The automated mode, was the mode primarily used during the NEAT STARC-ABL controls test campaign. In automated mode, the STARC-ABL propulsion system model and integrated controller compute the torque commands that are supplied to the motors. The user can select a test profile which contains controller settings along with time-varying values of PLA, Mach number, altitude, and ambient temperature. The final potential state of the machine is the "Fault" state. When an inverter hardware or communication fault occurs, a transition to the "Fault" state occurs and takes precedence over any state transition. An entry into this state triggers the inverters to be disabled, and thus halts any test in progress while stopping any motor

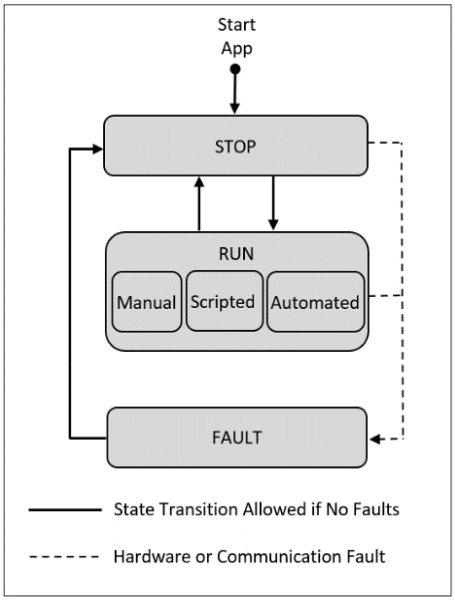

Figure 7: High-level State Machine Diagram

from spinning. The faults must be acknowledged and cleared before transitioning out of the "Fault" state. The state of the machine is implemented using Simulink Stateflow.

Communication between the dSPACE SCALEXIO real-time application and the motor inverter hardware occurs over Controller Area Network (CAN) bus interfaces. The inverters are configured to receive torque commands and supply motor speed feedback signals in addition to other motor and inverter feedback parameters. During NEAT testing, the dSPACE SCALEXIO system performs data acquisition and is responsible for archiving the STARC-ABL simulation parameters as well as inverter parameters provided over CAN bus communication.

V. Test Matrix

The test matrix for the NEAT STARC-ABL controls test consists of the following test card types: throttle profile test cards, mission profile test cards, and simulated abrupt performance degradation test cards. Each of these test card types and their associated test results are further discussed in the subsections below.

A. Throttle Profile Test Cards

Throttle profile test cards are conducted at simulated constant altitude and Mach number flight conditions spanning the STARC-ABL flight envelope. These throttle profile test cards were approximately six minutes in duration and subjected the system to PLA time histories consisting of gradual up and down ramps, stair steps up and down, and a single step up and down, all between idle and full power PLA settings. The purpose of these test cards is to verify that the developed control system can maintain desired system response and operability as the dynamics of the STARC-ABL changes throughout the operating envelope. In addition to executing the throttle profile test cards under nominal (undegraded) health conditions, these same test cards were also executed under 50% (midlife) and 100% (end-of-life (EoL)) simulated degradation conditions to assess the robustness of the control design. This is performed by adjusting health parameter inputs supplied to the STARC-ABL T-MATS model that simulates degradation of the efficiency and flow capacity of the turbomachinery components of the turbofans and tailfan.

B. Mission Profile Test Cards

Mission profile test cards are approximately 70 minutes in duration and subject the STARC-ABL control design to the altitude, Mach number, and PLA variations of full-flight profiles. This includes a 900 nautical mile (nm) reference mission and a mission profile based on actual flight data. The 900 nm reference mission is a shorter "economic" mission profile that was used in addition to a longer 3500 nm design reference mission in Ref. [5] to assess the overall efficiency of the STARC-ABL. The actual mission profile consists of altitude, Mach number, and PLA profiles based on actual data from a 70-minute flight acquired from the NASA Ames DASHLink website [17]. Mission profiles are run under both nominal and degraded conditions.

C. Simulated Abrupt Performance Degradation Test Cards

The simulated abrupt performance degradation test cards introduced individual step changes in the health condition of the two turbofans and the tailfan (i.e., nominal to midlife, midlife to end-of-life, and nominal to end-of-life step changes). The purpose of these test cards is two-fold. First, it allows the robustness of the control design to abrupt performance changes to be assessed. Additionally, it enables the acquisition of data for assessing subsystem interrelationships inherent within the STARC-ABL propulsion system architecture. Furthermore, it facilitates the development of health monitoring strategies for diagnosing the occurrence of events impacting STARC-ABL subsystem performance [18].

VI. Test Results

Testing of the STARC-ABL control design occurred at the NEAT facility in the summer of 2022. Select results from this testing are presented in the subsections below.

A. Throttle Profile Test Results

An illustration of the throttle profile test results for the sea-level-static (SLS) condition and a cruise condition set at 39,000 feet and a Mach number of 0.785 are shown in Fig. 8 and Fig. 9. The STARC-ABL's two geared turbofans operate symmetrically and thus only results from turbofan 1 are provided. Parameters shown include full-scale (unscaled) rotor speeds, stall margins, net thrust, fuel flow rate, motor torque, and generator torque. Each figure shows actual full-scale experimental results obtained during NEAT testing (thick cyan lines) compared against pre-test simulation predictions (thin red lines). The tailfan and turbofan LP speeds shown in the figures are filtered values obtained via the low-pass filter mentioned in Section IV.B. At the SLS condition, the system produces more net thrust

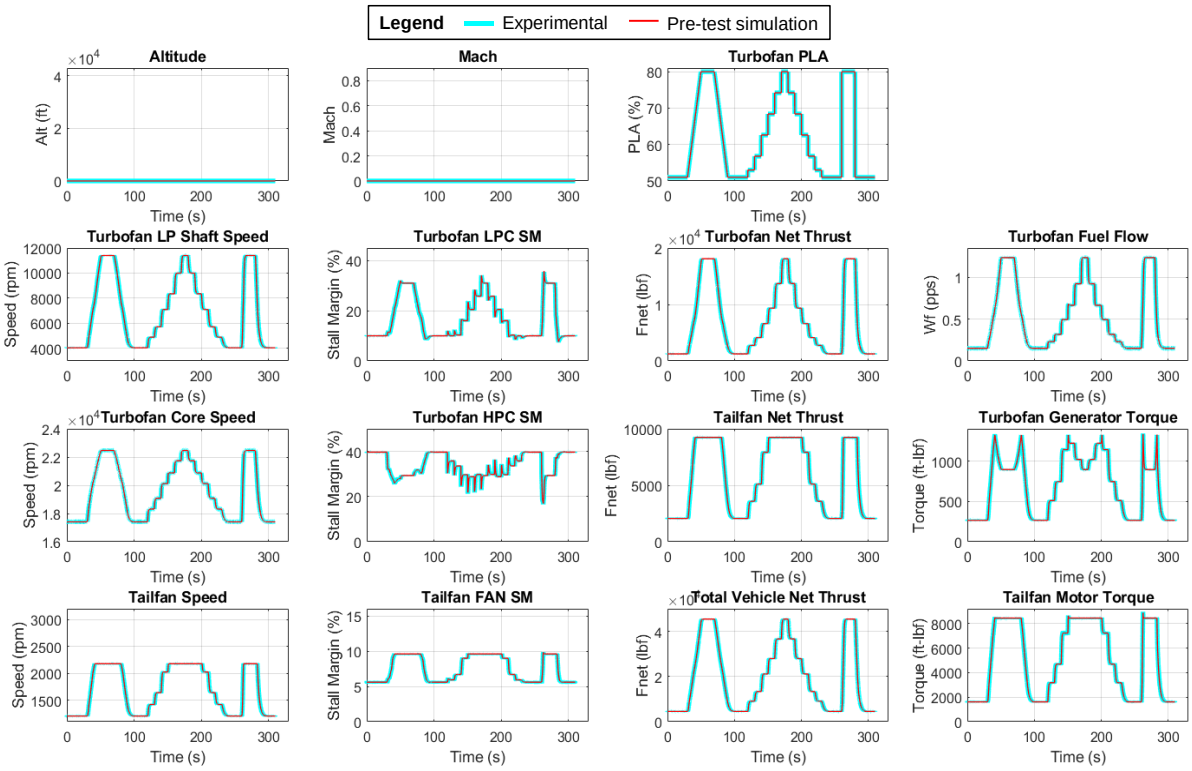

Figure 8. Throttle Profile Test Results – Sea Level Static Conditions

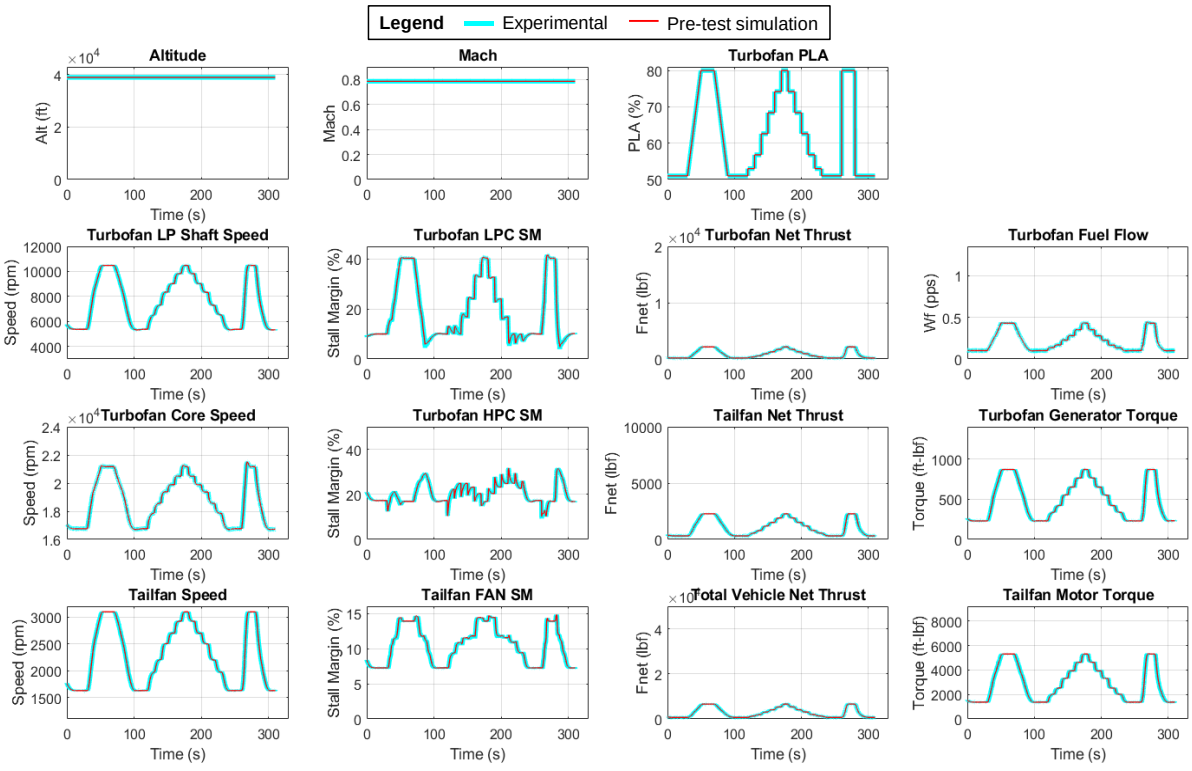

Figure 9. Throttle Profile Test Results – 39,000 Feet, 0.785 Mach

and consumes more fuel compared to the cruise flight condition, which is expected. At SLS the 3500hp maximum power limit of the tailfan motor is encountered at a PLA setting of approximately 67 degrees. This results in tailfan speed, net thrust, motor torque, and stall margin all plateauing at fixed values while turbofan parameters continue to change with increasing PLA as shown in Fig. 8. For the 39,000 feet 0.785 Mach data shown in Fig. 9, the 3500hp tailfan motor limit is not encountered given that less power is required to drive the tailfan at higher altitudes. In this case, both the tailfan and turbofan parameters continue to change with increasing PLA. Another difference between the SLS and cruise conditions is the dynamic response of the closed-loop system to PLA changes. At cruise, the control system is designed to respond more slowly to PLA changes. This is necessary to ensure adequate compressor stall margin is maintained during transients at higher altitude where there is less mass flow available to accelerate or decelerate the engine. In both figures, the agreement between experimental and pre-test predictions is very good.

Figure 10 shows a comparison of nominal and degraded EoL results at the 39,000 feet 0.785 Mach condition. Here, only the ascending portion of the PLA stairstep profile test cards is shown. Since the control system is designed to hold a target turbofan LP shaft speed and tailfan speed, those parameters are nearly identical for the nominal and EoL conditions. Net thrust produced by the turbofans and tailfan is also very similar for the two conditions. Noticeable differences are that the EoL condition results in increased turbofan core speed and fuel flow rate along with a reduction in low pressure compressor (LPC) and high pressure compressor (HPC) stall margin. EoL degradation also results in an increase in the required amount of tailfan motor torque and a slight increase in tailfan stall margin. Once again, the experimental test results are found to be in good agreement with pre-test simulation predictions. PLA profile test cards under midlife and EoL degradation conditions were run at a range of altitude and Mach flight conditions spanning the STARC-ABL flight envelope. In all cases, system operability was maintained and no compressor stall events occurred, thus demonstrating the robustness of the developed control system to function under both nominal health conditions as well as these representative levels of turbomachinery degradation.

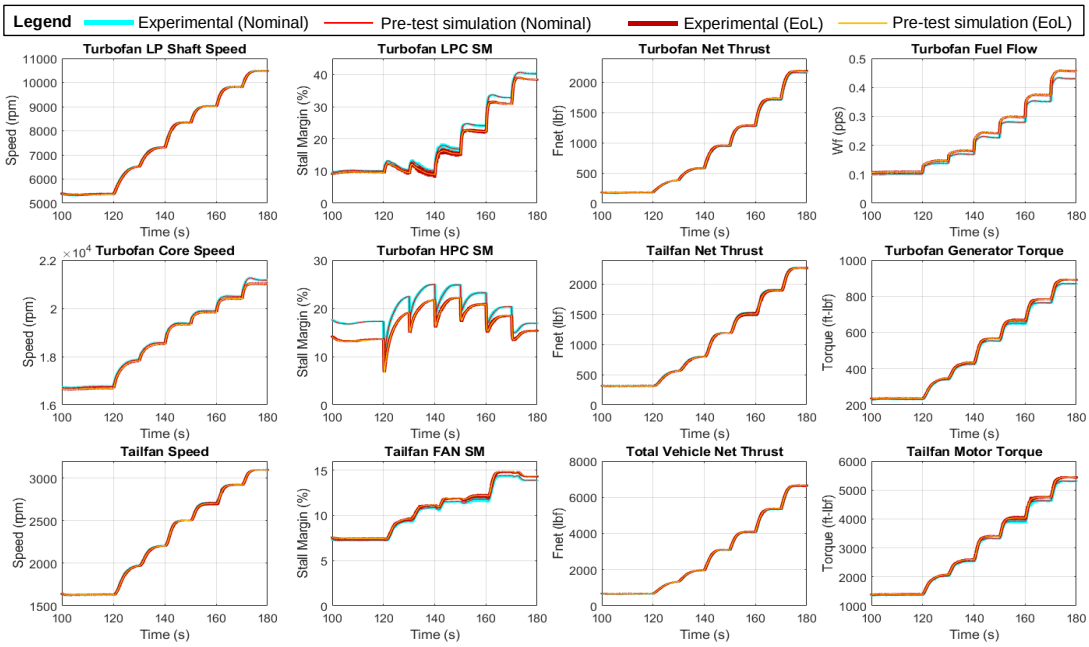

Figure 10. Throttle Ascending Stair Step Results – 39,000 Feet, 0.785 Mach (Nominal and EoL Degradation)

B. Mission Profile Test Results

Mission profile results for the 900 nm reference mission and the actual flight data mission are shown in Fig. 11 and Fig. 12, respectively. The 900 nm reference mission exhibits relatively limited PLA changes. Conversely, the Fig. 12 profile is based on actual aircraft flight data and exhibits considerably more variability in PLA, particularly during the descent phase of the flight profile. In both cases NEAT experimental results and pre-test simulation predictions are found to exhibit good agreement. In addition to running the mission profile test cards under nominal health conditions as shown in Figs. 11 and 12, these same test cards were repeated under EoL degradation conditions. Although not shown in this paper, experimental results and pre-test simulation predictions for those degraded cases exhibit good agreement as well. In all mission profile cases, including nominal and EoL health conditions, the STARC-ABL system controller performed as intended without issue. These results are very encouraging as they

further demonstrate the robust performance of the control design when subjected to realistic variations in flight condition, PLA movements, and degradation.

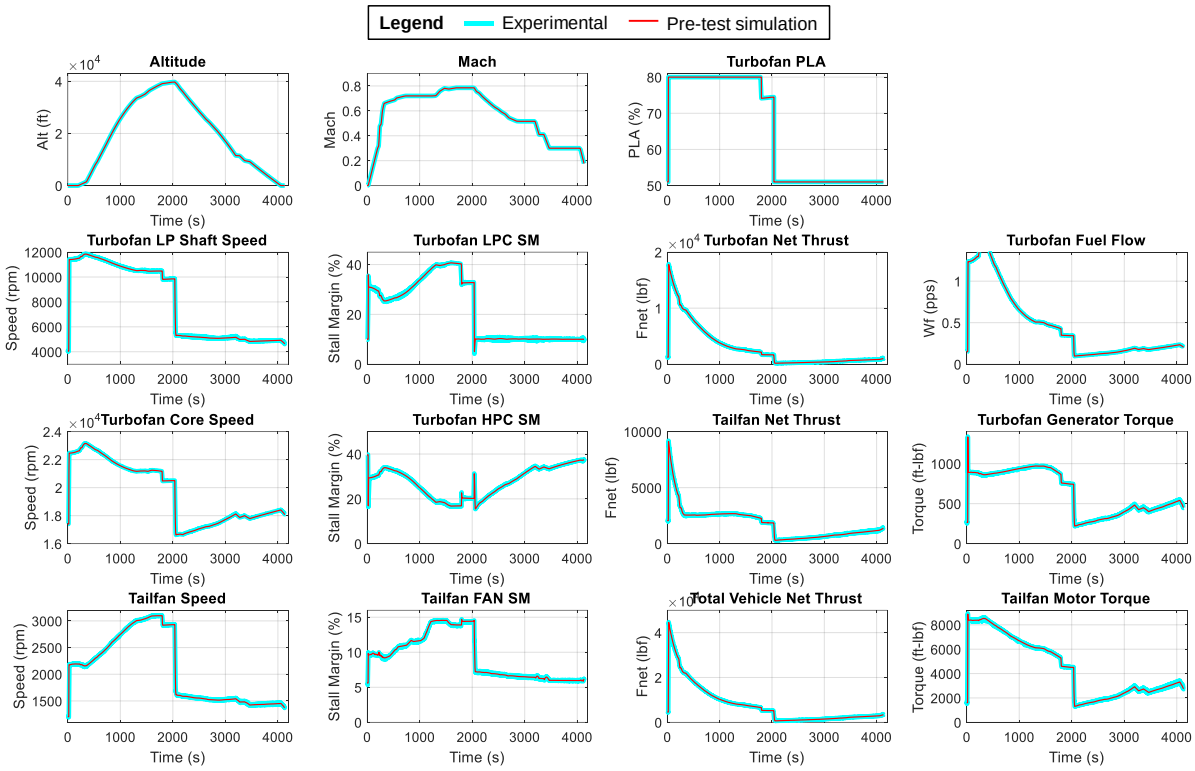

Figure 11. 900 Nautical Mile Economic Mission Results

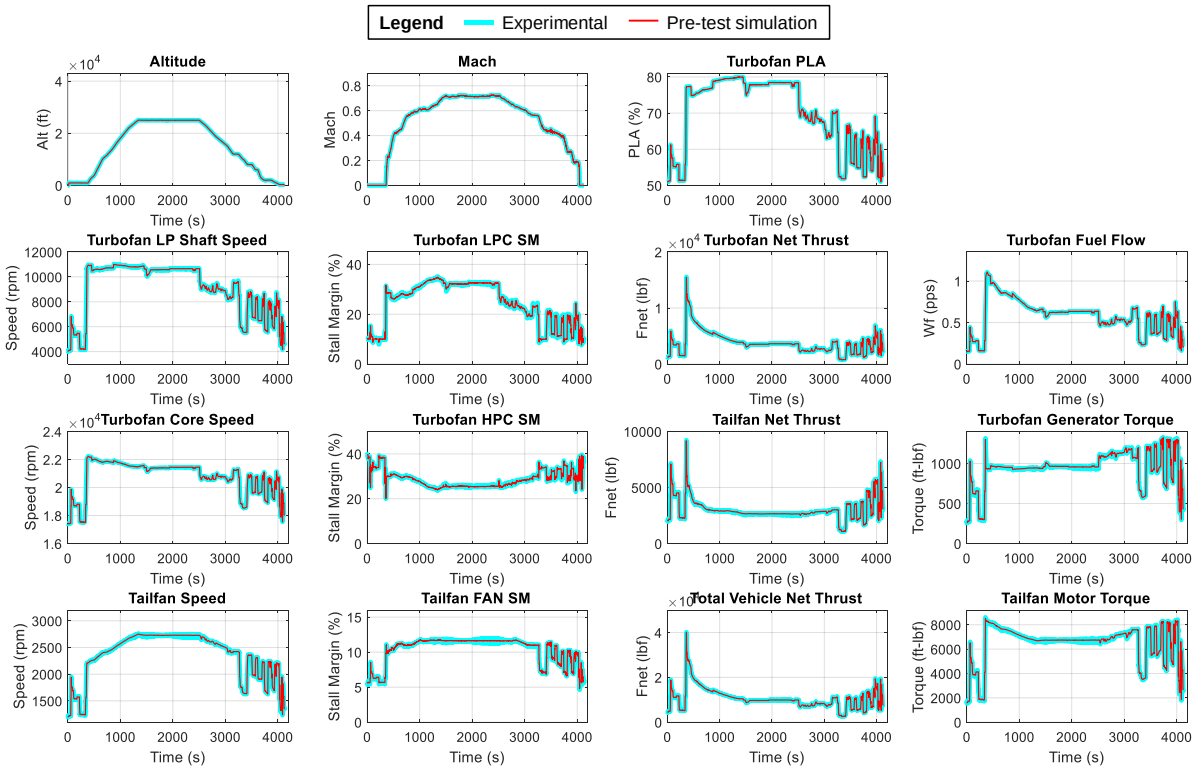

Figure 12. Actual Mission Profile Results

C. Simulated Abrupt Performance Degradation Test Results

The simulated abrupt performance degradation test cards introduce turbomachinery subsystem degradation changes in accordance with the time history profile shown in Fig. 13. Over the approximately 8-minute profile, step changes from nominal to midlife, midlife to EoL, and nominal to EoL levels of degradation are introduced and removed from each subsystem in isolation starting first in the tailfan, then turbofan 1, and finally turbofan 2. These abrupt step increases in degradation levels are simulated by simultaneously changing all health parameter settings within an individual subsystem. Such changes may be considered representative of events causing abrupt performance shifts in the system.

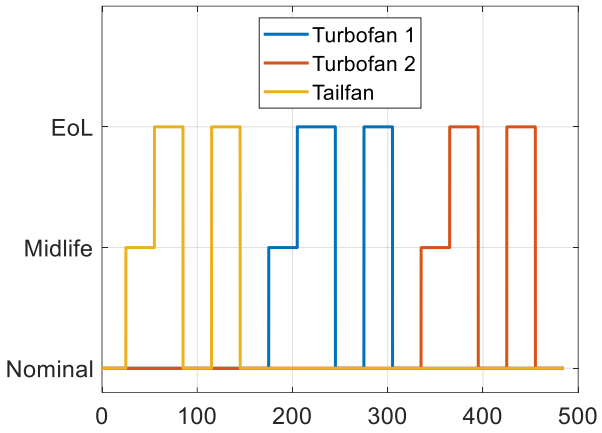

Figure 13. Abrupt Fault Test Card - Subsystem Degradation Levels

Abrupt performance degradation test card results for the 20k feet 0.6 Mach flight condition are shown in Fig. 14. Degradation changes within the individual turbofans are readily apparent in core speed, fuel flow rate and exhaust gas temperature (EGT) parameters. Tailfan degradation results in changes in tailfan exhaust temperature and the amount of motor torque required to hold tailfan speed at its setpoint. Of particular noteworthiness is the effect tailfan degradation has on the operation of the two turbofans. This is illustrated in the 25s to 145s portion of each plot. Here, notable increases in generator torque occurs, which results in increased turbofan core speed, fuel flow rate and EGT. This is due to the aft-to-forward coupling in the STARC-ABL architecture where tailfan degradation causes an increase in tailfan motor torque/power demand, which in turn requires additional turbofan generator power extraction to hold bus voltage constant.

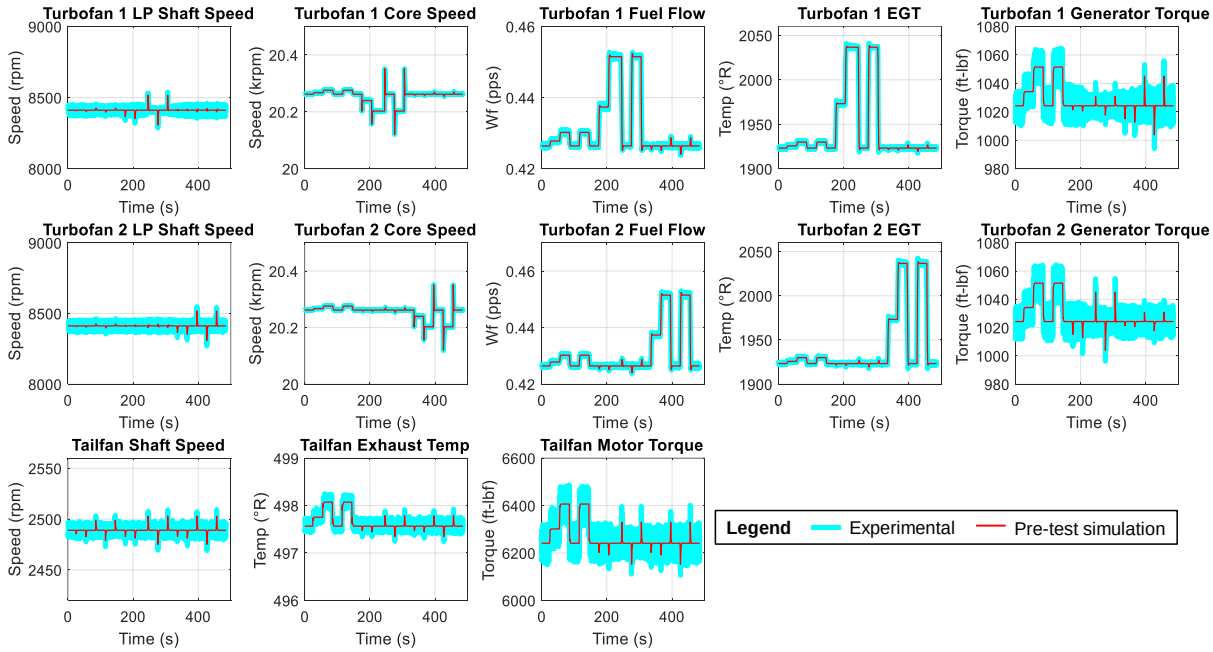

Figure 14. Simulated Abrupt Performance Degradation Test Results – 20k Feet, 0.6 Mach Flight Condition

The simulated abrupt performance degradation test results demonstrate the robust nature of the integrated control design in dealing with performance related shifts of this magnitude. The baseline control is found to maintain suitable system operability without the need for modification. More severe failure events, such as the complete failure of an

individual subsystem, would pose more serious consequences. For severe events, reversionary control modes will be necessary to allow continued operation of the propulsion system in the presence of the failure. Some past reversionary control studies have been performed for the STARC-ABL propulsion system [19,20]. Follow-on reversionary control development work incorporating the integrated control design strategy is recommended.

D. Summary of Test Cards Completed

During the NEAT STARC-ABL controls test campaign, a total of 140 test cards were executed and approximately 15 hours of test data were collected. To maintain a reasonable page length, only a portion of the NEAT STARC-ABL controls test results are included in this conference paper. A high-level summary of the test cards performed is provided in Fig. 15 where the various test card runs are plotted against the altitude versus Mach flight envelope of the STARC-ABL. This testing verified that the developed control strategy was able to maintain system operability throughout the flight envelope when subjected to PLA input transients under both nominal and degraded operating conditions.

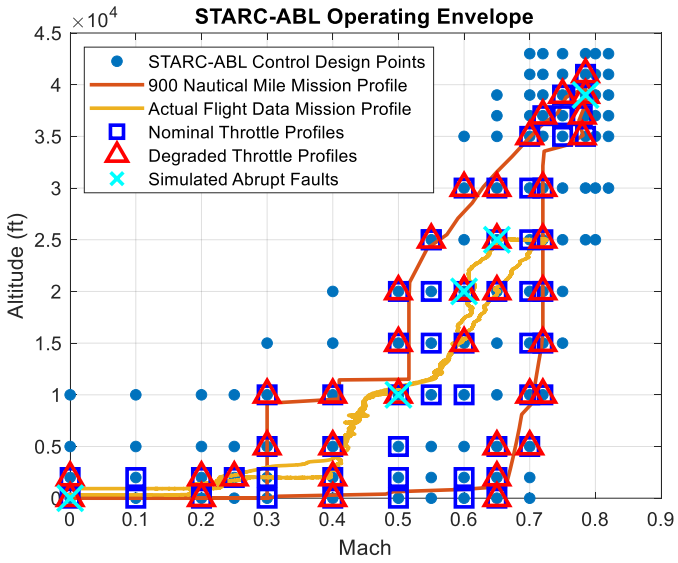

Figure 15. Summary of Test Cards Completed

VII. Conclusions

The NEAT STARC-ABL controls test demonstrated the successful implementation of an integrated control strategy for coordinating the operation of distributed partial turboelectric subsystems during transients throughout the flight envelope. The applied control strategy allowed the turbofan control design problem to be transformed into a single-input single-output problem; a form that readily lends itself to classical linear control design and analysis techniques. A similar coupled control design strategy may also be useful for other distributed electrified aircraft propulsion architectures that exhibit coupling between subsystems. During hardware-in-the-loop testing at the NEAT facility, the STARC-ABL control system performed as expected and no control system or turbomachinery operability issues were encountered. This included testing under both nominal health turbomachinery and simulated turbomachinery degradation, which demonstrated the robustness of the technique. Follow-on work to allow the control technique to function in the presence of subsystem failures is recommended, including the development of reversionary control modes to assist in the mitigations of such failures.

Acknowledgments

This work was conducted under the NASA Advanced Air Vehicles Program, Advanced Air Transport Technology Project, Power and Propulsion Subproject. The authors graciously acknowledge the tremendous support provided by the NEAT facility engineers and technicians that made this research effort possible.

References

[1] National Aeronautics and Space Administration, (2022), "Sustainable Flight National Partnership," https://www.nasa.gov/aeroresearch/sustainable-aviation-np/

[2] Jansen, R.H., Bowman, C., Jankovsky, A., Dyson, R., Felder, J., (2017), "Overview of NASA Electrified Aircraft Propulsion Research for Large Subsonic Transports," AIAA-2017-4701, *AIAA Propulsion and Energy Forum*, Atlanta, GA, July 10-12.
[3] Felder, J.L., (2015), "NASA Electric Propulsion System Studies," presentation, *5th EnergyTech 2015*, Cleveland, OH, Nov. 30 – Dec 2.
[4] National Academies of Sciences, Engineering, and Medicine. 2016. Commercial Aircraft Propulsion and Energy Systems Research: Reducing Global Carbon Emissions. Washington, DC: The National Academies Press. https://doi.org/10.17226/23490.
[5] Welstead, J.R., Felder, J.L., (2016), "Conceptual Design of a Single-Aisle Turboelectric Commercial Transport with Fuselage Boundary Layer Ingestion," AIAA 2016-1027, *AIAA SciTech Forum*, *54th AIAA Aerospace Sciences Meeting*, San Diego, CA, January 4-8.
[6] Felder, J. L., Schnulo, S. L., Tong, M. T., Berton, J. J., Thacker, R. P., Haller, W. J. (2022), "An Updated Assessment of Turboelectric Boundary Layer Ingestion Propulsion Applied to a Single-Aisle Commercial Transport," *AIAA SciTech Forum and Exposition*, San Diego, CA, January 3-7.
[7] Connolly, J. W., Chapman, J. W., Stalcup, E. J., Hunker, K. R., Chicatelli, A. K., and Thomas, G. L., (2018), "Modeling and Control Design for a Turboelectric Single Aisle Aircraft Propulsion System," AIAA-2018-5010, *AIAA/IEEE Electric Aircraft Technologies Symposium (EATS)*, Cincinnati, Ohio, July 9-11.
[8] Connolly, J., and Stalcup, E., (2017), "Dynamic Modeling, Controls, and Testing for Electrified Aircraft," In *Energy Technology (EnergyTech) Conference*, Cleveland, Ohio, October 31.
[9] Kratz, J.L, Thomas, G.L., (2019), "Dynamic Analysis of the STARC-ABL Propulsion System," AIAA-2019-4182, *AIAA Propulsion and Energy Forum*, Indianapolis, Indiana, August 22-24.
[10] Simon, D.L., Bianco, S.J., Horning, M.A., (2023), "Integrated Control Design for a Partially Turboelectric Aircraft Propulsion System," ASME-GT2023-100921, *ASME Turbo Expo Conference*, Boston, MA, June 26-30, [Accepted]
[11] Haglage, J. M., Brown, T. W., "NASA Electric Aircraft Testbed (NEAT) Reconfiguration to Enable Altitude Testing of Megawatt-Scale Electric Machines," *AIAA Propulsion and Energy Forum*, New Orleans, LA, 2020.
[12] Jaw, L., & Mattingly, J., (2009), "Aircraft Engine Controls," New York, NY, USA: American Institute of Aeronautics and Astronautics.
[13] Lytle, J., Follen, G., Naiman, C., Evans, A., Veres, J., Owen, K., Lopez, I., (2000), "Numerical Propulsion System Simulation (NPSS) 1999 Industry Review," NASA/TM-2000-209795, August.
[14] Chapman, J.W., Lavelle, T.M., May, R.D., Litt, J.S., Guo, T-H., (2014), "Toolbox for the Modeling and Analysis of Thermodynamic Systems (T-MATS) User's Guide," NASA/TM-2014-216638, January.
[15] Chapman, J.W., Litt, J.S., (2018), "An Approach for Utilizing Power Flow Modeling for Simulations of Hybrid Electric Propulsion Systems," AIAA-2018-5018, *AIAA Propulsion and Energy Forum*, Cincinnati, OH, July 9-11.
[16] Bianco, S. J., Simon, D. L., (2023), "Control and Scaling Approach for the Emulation of Scaled Dynamic Torque Loads," *AIAA Aviation/Electrified Aircraft Technology Symposium (EATS),* San Diego, CA, June 12-16.
[17] DASHlink—Sample Flight Data, (2012), available online: https://c3.nasa.gov/dashlink/resources/664/ (accessed on 12 October 2022).
[18] Simon, D. L., Thomas, R., Dunlap, K. M. (2022), "Considerations for the Extension of Gas Path Analysis to Electrified Aircraft Propulsion Systems," *Journal of Engineering for Gas Turbines and Power*, 144(3).
[19] Simon, D. L., and Connolly, J. W., (2020), "Electrified Aircraft Propulsion Systems: Gas Turbine Control Considerations for the Mitigation of Potential Failure Modes and Hazards," ASME-GT2020-16335, *ASME Turbo Expo Conference*, Virtual, Online, September 21-25.
[20] Kratz, J. L., and Simon, D. L., (2022), "Failure Modes and Mitigation Strategies for a Turboelectric Aircraft Concept with Turbine Electrified Energy Management," AIAA 2022-1191, AIAA SciTech Forum, San Diego, CA, January 3-7.